Physiological dynamic compression regulates central energy metabolism in primary human chondrocytes

Authors: Daniel Salinas, Brendan M. Mumey, and Ronald K. June

The final publication is available at Springer via https://dx.doi.org/10.1007/s10237-018-1068-x.

Salinas, Daniel, Brendan M. Mumey, and Ronald K. June. "Physiological dynamic compression regulates central energy metabolism in primary human chondrocytes." Biomechanics and Modeling in Mechanobiology 18 (February 2019): 69-77. DOI:10.1007/s10237-018-1068-x.

Biomechanics and Modeling in Mechanobiology manuscript No.
(will be inserted by the editor)

Physiological Dynamic Compression Regulates Central Energy Metabolism in Primary Human Chondrocytes

Daniel Salinas · Brendan M. Mumey · Ronald K. June

Received: date / Accepted: date

Abstract Chondrocytes use the pathways of central metabolism to synthesize molecular building blocks and energy for homeostasis. An interesting feature of the *in vivo* chondrocyte environment is the cyclical loading generated in various activities (*e.g.* walking). However, it is unknown if central metabolism is altered by mechanical loading. We hypothesized that physiological dynamic compression alters central metabolism in chondrocytes to promote production of amino acid precursors for matrix synthesis. We measured the expression of central metabolites (*e.g.* glucose, its derivatives, and relevant co-factors) for primary human osteoarthritic chondrocytes in response to 0-30 minutes of compression. To analyze the data, we used principal components analysis and ANOVA simultaneous components analysis, as well as metabolic flux analysis. Compression induced metabolic responses consistent with our hypothesis. Additionally, these data show that chondrocyte samples from different patient donors respond differently to compression. Most important, we find that grade IV osteoarthritic chondrocytes are capable of synthesizing non-essential amino acids and precursors in response to mechanical loading. These results suggest that further advances in metabolic engineering of chondrocyte mechanotransduction may yield novel translational strategies for cartilage repair.

This study was funded by the National Science Foundation (NSF 1342420 and 1554708.)

Ronald K. June II
Montana State University
PO Box 173800
Bozeman, MT 59717-3800
Tel.: +1-406-994-5941
Fax: +1-406-994-6292
E-mail: rjune@montana.edu

Keywords osteoarthritis · cartilage repair · mechanotransduction · chondrocyte · systems biology · metabolic flux analysis

1 Introduction

Central metabolism is the primary set of pathways by which cells harvest energy and other molecular building blocks. These pathways include glycolysis, the pentose phosphate pathway, and the tricarboxylic acid cycle (Fig. 1). From these pathways, cells can generate both adenosine triphosphate (ATP) to fuel cellular processes and various precursors to non-essential amino acids. Historically, chondrocytes have been considered glycolytic cells, but recent data suggest that chondrocytes utilize both glycolytic and oxidative pathways (Coleman et al 2016; Griffin et al 2012; Martin et al 2012; Zignego et al 2015; Blanco et al 2011).

Chondrocytes reside in a viscoelastic microenvironment (Alexopoulos et al 2005; Xu et al 2016). Everyday activities, such as walking, apply cyclical loads to chondrocytes that are transmitted through the pericellular matrix (PCM). Because of its viscoelastic nature, the chondrocyte PCM is capable of both storing and dissipating the mechanical energy generated in *in vivo* activity. However, it is unknown if cyclical mechanical loading to physiological levels can affect central metabolism in chondrocytes. Therefore, the objective of this study was to examine changes in the metabolites of central metabolism for chondrocytes subjected to physiological compression.

We hypothesized that physiological dynamic compression would alter central metabolism in chondrocytes to promote production of amino acid precursors. Recent studies (Coleman et al 2016; Brouillette et al

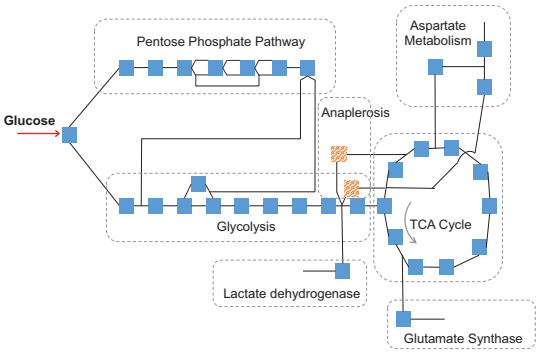

Fig. 1 (Map of central energy metabolism. Each square represents a modeled reaction, and lines represent metabolites, most of which are detected experimentally. Pathways included are glycolysis, pentose phosphate pathway, and the citric acid cycle (with anaplerotic reactions), and reactions in aspartate, glutamine, and lactate metabolism that share metabolites with these pathways. Electron transport chain reactions not shown for simplicity, but are included in the model.

2014) have shown injurious loading of chondrocytes is inimical to respiration, drawing a link between central metabolism and mechanical stimulus. However, we hypothesized that moderate, physiological stimulus promotes cartilage homeostasis, *i.e.* that moderate physical activity triggers tissue maintenance. Because the PCM is composed of proteins such as Type VI collagen and FGF (Wilusz et al 2014; Vincent et al 2007), production of amino acid precursors through compression-induced responses in central metabolism has the potential to maintain cartilage homeostasis.

To test this hypothesis, we applied cyclical compression to primary human chondrocytes encapsulated in physiologically stiff agarose. To examine changes in central metabolism, we performed metabolomic profiling and analyzed the expression of 37 metabolites including glucose and its derivatives. To assess the general regulation of central metabolism by compression, we performed principal components analysis (PCA) and ANOVA-simultaneous components analysis on the metabolite expression data. To examine rates of production of amino acid precursors, we used metabolic flux analysis with a recently developed stoichiometric model (Salinas et al 2017).

The results show that compression induces substantial changes in central energy metabolites after just 15 or 30 minutes. Furthermore, production of amino acid precursors increases after dynamic compression. These results demonstrate that osteoarthritic chondrocytes can alter their central metabolism in response to applied compression. Furthermore, chondrocytes increase production of precursors to non-essential amino acids suggesting a mechanistic link between compression and maintenance of cartilage homeostasis that involves central metabolism.

2 Methods

This study involves additional analyses of previously-published data (Zignego et al 2015). These data come from primary human chondrocytes harvested from femoral heads of total hip arthroplasty patients under an IRB-exempt protocol.

2.1 Chondrocyte Encapsulation and Compression

The methodology for compressing chondrocytes has been previously published (Zignego et al 2014). Briefly, chondrocytes were harvested from five patients undergoing joint replacement surgery. All had stage IV osteoarthritis. Chondrocytes were isolated, expanded for one passage, and subsequently encapsulated in agarose gel of physiological stiffness to ensure transmission of compressive loads. After three days of equilibration in the gel, they were subjected to dynamic compression for up to 30 minutes. The compression was designed to simulate the human gait (1.1 Hz, ∼5% strain with 1.9% amplitude). Samples were collected at 0 (control, no compression), 15, and 30 minutes. We used independent samples from five donors, and had three to five replicates per donor.

2.2 Metabolite Extraction

The methodology for quantifying metabolites from central metabolism has been previously published (Jutila et al 2014). In summary, chondrocytes were flash-frozen after compression. Metabolites were extracted and quantified using high performance liquid chromatography coupled with mass spectrometry (HPLC-MS). A targeted analysis yielded intensities for 37 known metabolites in central metabolism.

2.3 Components Analysis

Metabolomic data describes an organism's metabolic state in terms of the abundance of each of its metabolites. To quantify chondrocyte response to compression, we applied principal components analysis (PCA) and subsequently ANOVA-Simultaneous Components Analysis (ASCA) to this data. ASCA is an extension of

PCA, whereby each datum is interpreted as the sum of the effects of factors defined by the experimental design. We applied ASCA to rigorously analyze any changes induced by compression time, independent of all other factors, on the observed metabolite expression patterns once PCA had shown this effect to be roughly linear.

To apply PCA, the data were compiled into a matrix, $\mathbf{X}$, with a row for each sample and a column for each metabolite. The dimensions of $\mathbf{X}$ in this study were therefore 69×37, since a total of 69 samples were harvested and, for each, 37 metabolites were measured. The entry at row i and column j is the abundance of metabolite j in sample i as measured by HPLC-MS. The principal components, *i.e.* the axes along which the data varied, were then computed as the eigenvectors of the covariance matrix of the mean-centered data (Ten Berge et al 1992).

As mentioned, ASCA defines each value in $\mathbf{X}$ as a sum of the effects of the factors (also referred to as "treatments") in the experiment that generated the data. In this study, the factors are the the length of time the chondrocyte was compressed (*e.g.* 0, 15, or 30 minutes) and the donor it was taken from; formally, the abundance of metabolite j in sample i is

$$x_{ij} = \mu + e_{di} + e_{ti} + e_{tdi} + \epsilon, \tag{1}$$

where μ is the mean abundance over all samples, e_{di} is the effect of the donor sample i was taken from, e_{ti} is the effect of the time t sample i was compressed, e_{tdi} is the effect of the interaction between donor and time (which can be interpreted as donor sensitivity to compression), and ϵ is random error. The terms in eq. 1 are defined by

$$\begin{aligned} e_{di} &= \mu_d - \mu, \\ e_{ti} &= \mu_t - \mu, \\ e_{tdi} &= \mu_{td} - e_d - e_t - \mu, \end{aligned} \tag{2}$$

and finally ϵ can be computed from eq. 1 once the other terms have been established. The mean μ_d is the mean of all samples from donor d, and the mean μ_t is the mean of the samples compressed for time t. Eq. 1 yields a set of matrices,

$$\mathbf{X} = \mathbf{M} + \mathbf{T} + \mathbf{D} + \mathbf{I} + \mathbf{E}, \tag{3}$$

in the natural way, *i.e.* by computing the terms in eq. 1 for each x_{ij} in $\mathbf{X}$ and arranging each collection of terms into a matrix according to $\mathbf{X}$. There are several variations of ASCA (Timmerman and Kiers 2003), among them ASCA-P. We applied ASCA-P as in (Smilde et al 2005) using the accompanying code, which applies PCA to the matrices on the right hand side of eq. 3.

PCA and ASCA compute how metabolites shift together in the data. To illustrate, we consider the case where there are only three samples and two metabolites measured per sample. $\mathbf{X}$ is therefore a 3×2 matrix. Let the first row of $\mathbf{X}$ be [1 1], the second be [2 3], and the third be [3 5]. Let the time of compression for the first row be 10 minutes, the second 20 and the third 30. Then shift is easily computable: as the time of compression increases, the abundance of both metabolites increases. Specifically, the abundance of the first metabolite increases by 1 unit with each 10 minutes of compression, and the second increases by 2 units. So the data can be said to exhibit a shift of [0.1 0.2] over time, since multiplying this vector by the time yields the measured shift in abundance. PCA and ASCA yield profiles by expressing data points as a combination of the effects of the factors time and donor. Whereas in the previous example there is only one direction of change, any $\mathbf{X}$ with n columns can be expressed as the combination of up to n directions away from the overall mean. PCA and ASCA find the directions that most closely preserve the variation in $\mathbf{X}$ if fewer than n are considered. The significance of the trends detected were assessed via a label permutation study (Vis et al 2007).

2.4 Systems Analysis

Metabolic flux analysis (MFA) expresses changes in metabolite abundances as the product of reactions in metabolic pathways occurring at specific rates. Formally, the changes in abundance $\mathbf{c}$ and the reaction rates $\mathbf{r}$ are related by

$$\mathbf{Sr} = \mathbf{c} \tag{4}$$

where $\mathbf{S}$ is the stoichiometric matrix. Given a stoichiometric matrix $\mathbf{S}$ and a set of changes $\mathbf{c}$, the reaction rates can be computed by solving the system for $\mathbf{r}$. In prior work, we created a stoichiometric matrix from the set of reactions that comprise central metabolism (Salinas et al 2017). Briefly, the stoichiometric matrix is used to compute the change in the abundance of a given metabolite from a set of reaction rates by summing the rates of all the reactions that produce that metabolite and subtracting the rates of the reactions that consume that particular metabolite. If the reactions produce or consume more than one unit, their rate is weighted accordingly. A stoichiometric matrix allows for the enforcement of conservation laws, balancing atoms, electrons, and protons (Stephanopoulos et al 1998).

In this study, $\mathbf{S}$ was compiled from the reactions in glycolysis, the tricarboxylic acid cycle (with accompanying anaplerotic reactions), pentose phosphate pathway, and the electron transport chain. Due to the high

abundance of lactate, glutamate, glutamine, aspartate and alanine in our samples, and their direct interaction with central metabolism, the reactions mediated by lactate dehydrogenase, aspartate oxidase, aspartate ammonia lyase, glutamate synthase, and aspartate decarboxylase were also incorporated. The stoichiometric matrix used in our study can be found in the supplementary material (File S1). The methodology used to solve for **r** is the same as our prior study (Salinas et al 2017).

Once a shift **c** has been computed, eq. 4 is used to compute the rates that most closely replicate that shift. We computed **r** for the shift caused by compression time according to ASCA and for the change with time observed in each individual donor. The **c** for these were calculated by subtracting the median sample compressed for 0 minutes from the median of the sample compressed for 30 minutes. These **r** were compared to the ASCA **r** to assess how closely individuals followed the aggregate trend. Further explanation of metabolic flux analysis can be found in the seminal text (Vallino and Stephanopoulos 1989).

3 Results

3.1 Principal Components Analysis

PCA revealed that the variation between donors (97% of the variation) is larger than the variation within donors induced by compression (3% of the variation, Fig. 2). Despite differing in base metabolite abundance, compression induced similar changes in abundance in almost all donors (Fig. 2). The first three principal components preserved 99% of the total variation, indicating that the three-axis representation of the data is fairly close to the original. Resolving the data along these three principal components showed that the axes of the first two principal components represent donor-dependent variation, with the third representing changes over time.

Analyzing only the samples belonging to a single donor at a time showed that samples that have been compressed tend to have a higher position along the third principal component axis than the samples that were not compressed, provided the comparison is between samples from the same donor (Figs. 2, 3B). The exception is donor 1, the the youngest (age 54 vs. 59, 60, 64, and 80) and only male donor. However, as discussed below, this donor's samples also responded noticeably and consistently to compression.

Changes induced by compression were associated with the third principal component in the data, indicating physiological compression regulates central metabolites as hypothesized. The compression time axis had loadings that showed negative coefficients for glucose, glutamate and aspartate, and positive coefficients for glutamine and pyruvate (Fig. 3A). As they are compressed, chondrocytes lose glucose, glutamate, and aspartate, and gain glutamine and pyruvate. Again, the exception to this is donor 1. Further interpretation is provided in §4. Donor 5, a 64 year old female, had the most pronounced separation along the compression time axis.

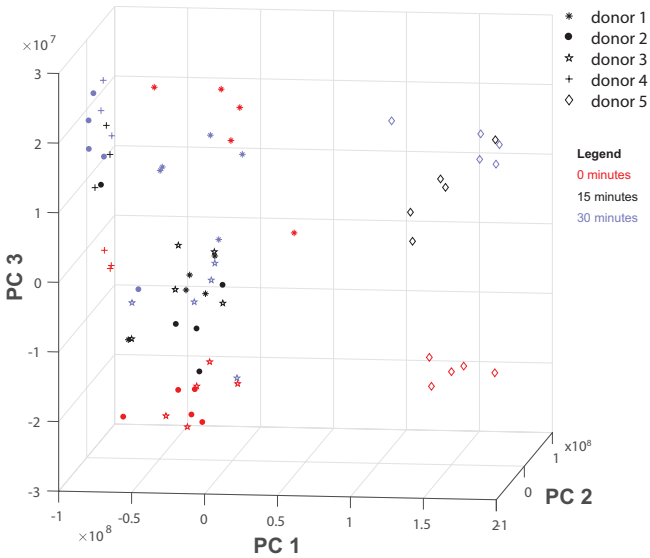

Fig. 2 Principal components analysis of donor data. Each point represents a sample (associated with a donor and time of compression and composed of 37 measurements) after projection onto the three principal axes of variation. Red, black, and blue samples have been compressed for 0, 15, and 30 minutes, respectively. PC1 captures the differences between donor 5 and the rest of the donors; PC2 and PC3 capture the variation between donors and across time. PC3 especially is associated with the direction of change across time. Samples compressed for a longer time are higher along axis PC3 than those compressed for a lesser time, if they are from the same donor.

3.2 ANOVA Simultaneous Components Analysis

While the third axis of PCA is associated with changes induced by compression, we applied ASCA to rigorously define what these changes are according to the ANOVA model. ASCA showed two principal axes (100% of time variance associated with them). The loadings for the first ASCA axis (89% variance) shared the negative coefficients for glucose and positive coefficients for glutamine that the third PCA axis had (Fig 3A). However, the aspartate and glutamate coefficients are positive. Also, the coefficient for proline is the third largest. This axis and the third PCA axis have a high correla-

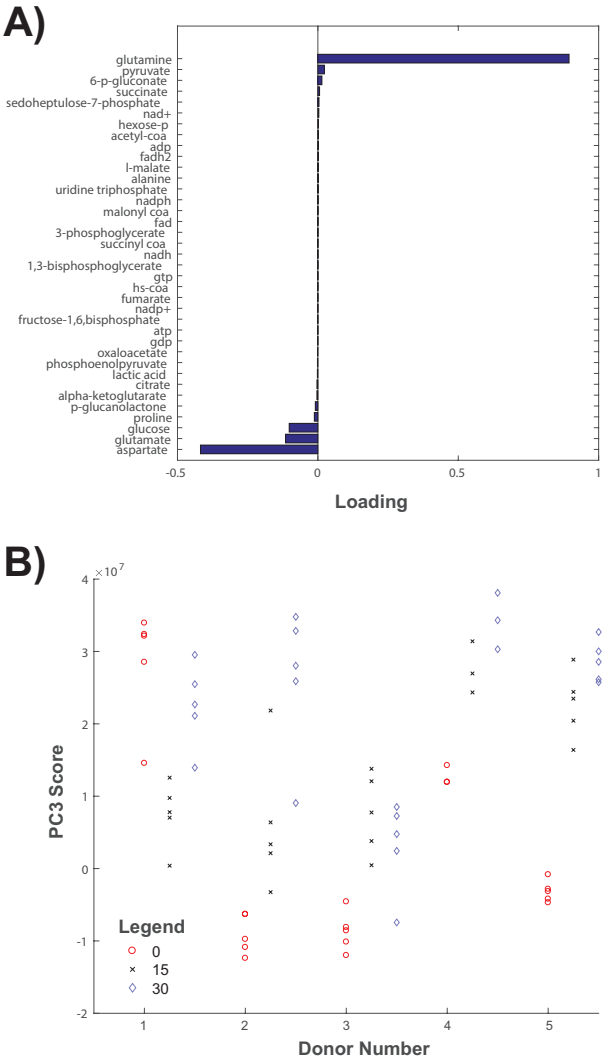

Fig. 3 (A) Loading values along PC3 for each metabolite, sorted from least (bottom) to greatest (top). (B) Data for donors 1-5 after projection onto the third principal component. Red, black, and blue samples represent samples compressed for 0, 15, and 30 minutes, respectively. Compressed samples tend toward the top, obtaining higher PC3 scores.

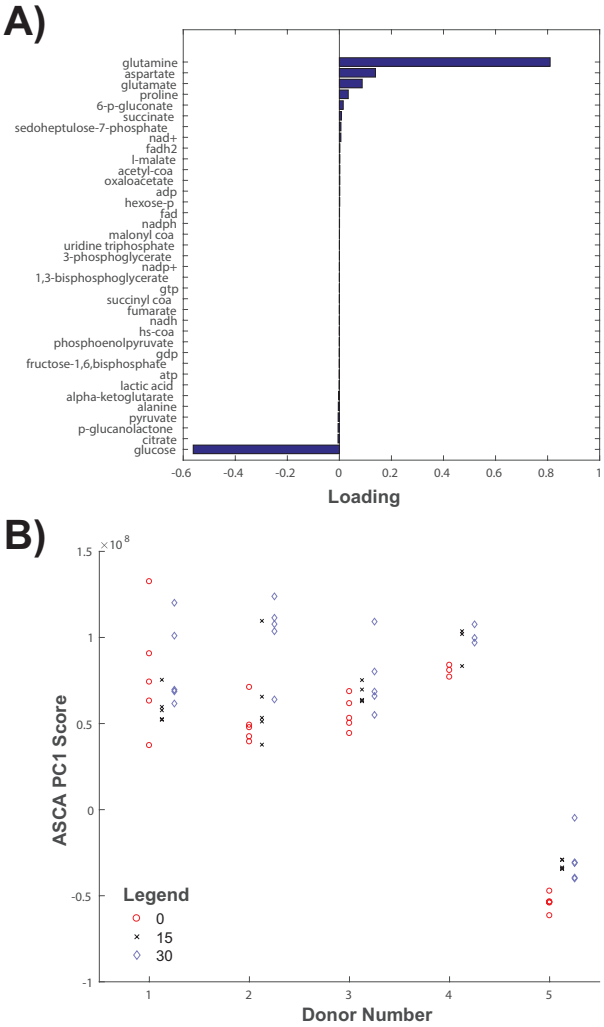

Fig. 4 (A) Loading for each metabolite along the first principal component computed by ANOVA-Simultaneous Components Analysis (ASCA PC1), sorted from least (bottom) to greatest (top). (B) Data for donors 1-5 after projection onto ASCA PC1 (vertical dimension). Red, black, and blue samples represent samples compressed for 0, 15, and 30 minutes, respectively. Compressed samples tend toward the top, obtaining higher ASCA PC1 scores.

tion (> 0.5) and similarly discriminate between non-compressed and compressed data (Figs. 4B, 5). This validates the third PCA axis as related to time of compression. However, the difference in the loadings for glutamate and aspartate show this axis captured additional sources of variation. As expected, after projection along the first ASCA principal component axis the compressed samples tend to receive higher scores than the uncompressed when comparing within each donor. The permutation study showed that the variation of compressed and uncompressed groups from the mean was much larger than could be expected by random variation due to small sample size, to high significance ($p < 0.05$). This indicates the populations are significantly different and that compression affects chondrocyte central metabolism.

3.3 Metabolic Flux Analysis

As discussed in §2, the changes in metabolite abundances allow us to infer the reaction rates that produced them using MFA. The change in abundances over time corresponding to the first ASCA axis requires high activities for glycolysis and the pentose phosphate pathway coupled with high conversion of ammonia lyase into fumarate, high conversion of malate to pyruvate, and high oxidation of aspartate (Fig. 6A). The rates that

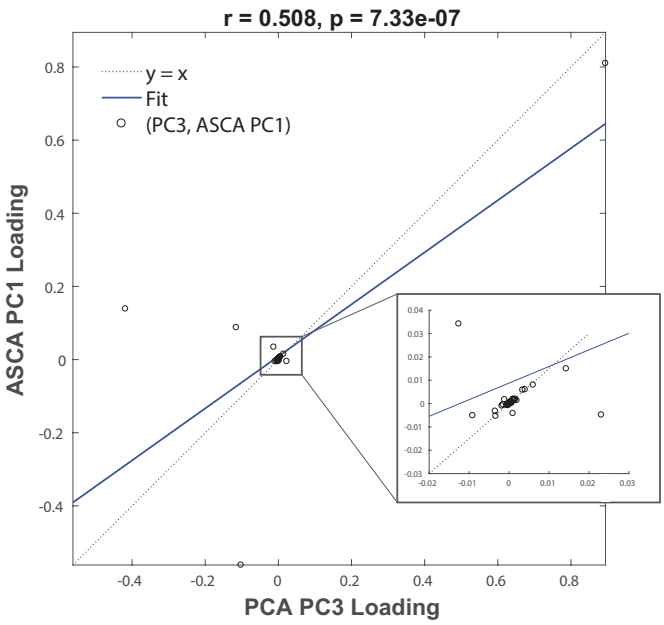

Fig. 5 Regression plot examining the similarity between the third principal component (PCA PC3) and the first principal component of time (ASCA PC1). The correlation coefficient is 0.508 ($p < 0.05$). For each metabolite, the PC 3 loading is the horizontal coordinate and the ASCA PC 1 loading is the vertical coordinate. The main discrepancies are aspartate, glutamate, and glucose.

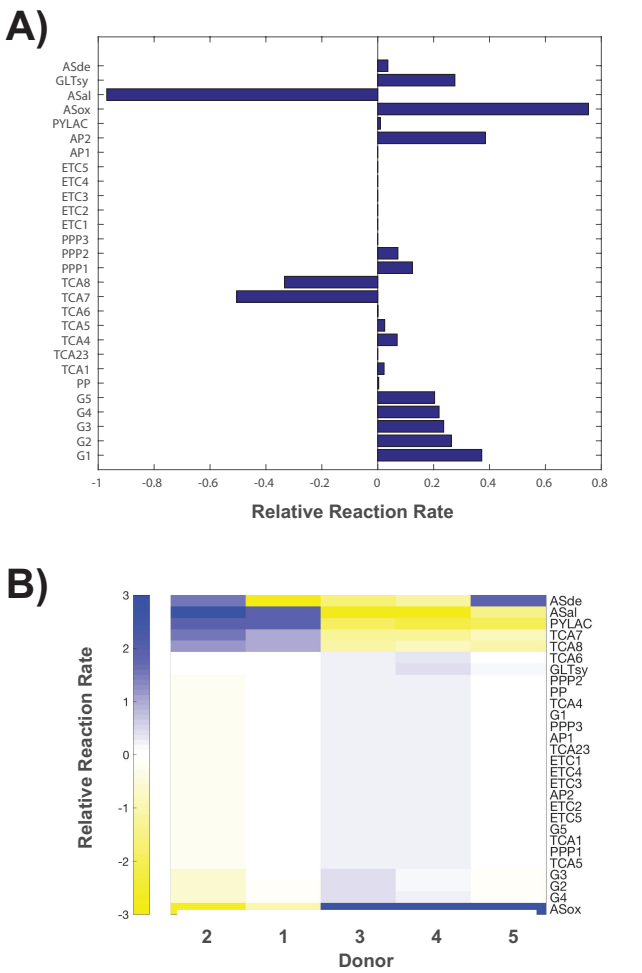

Fig. 6 (A) Reaction rates that generate the changes in metabolite abundances induced by compression. These rates match the changes calculated by ASCA. They rates are consistent with increased synthesis of aspartate, pyruvate, and ATP: all needed for protein synthesis as required by chondrocyte homeostasis. (B) Reaction rates for each donor, for the periods of 0-30 minutes of compression, calculated from the differences in the medians of the samples for each time point. These are consistent with the compression rates, demonstrating that the overall shift in metabolism within donors comes as a result of compression over time.

match the third PCA axis were almost identical to the ASCA rates (not shown). The rates calculated from the median samples for donors 3, 4, and 5 were consistent with the ASCA rates, showing that ASCA and PCA accurately infer the change in overall metabolomic profiles (Fig. 6B). The rates for the donors and times share two major clusters: one for donors 1 and 2 and the other for the other rates (Fig 5B). Donors 1 and 2 are the youngest and oldest donors, respectively. Further discussion of these rates is found in §4.

4 Discussion

The effect of physiological compression on the central metabolism of primary osteoarthritic chondrocytes can be quantified using targeted metabolomic data and interpreted via MFA. PCA and ASCA are tools that enable the researcher to aggregate changes in observed in individual metabolite abundances into axes of variation which summarize the correlated changes as movement in a single direction. While donor-dependent differences were larger than the differences in metabolism induced by compression, almost all donors reacted similarly to compression. The significance of this data is the demonstration that human osteoarthritic chondrocytes respond to physiological compression through central metabolism suggesting the potential for load-induced cartilage repair.

Under PCA, donor 5 was the most distinct. From the loadings of the first PCA axis, it is apparent that the difference between donor 5 and the others is due to a large abundance of glucose relative to the other donors (Fig. 2A). Samples from this donor also had lower relative aspartate and glutamate abundances. The higher glucose does not cause a difference in the nature of chondrocyte response to compression, as her samples separated well along the time of compression axes, *i.e.* PCA axis 3 and ASCA axis 1. Higher glucose abundance might have an effect on the sensitivity to com-

pression, however. After 15 minutes of compression, all of her samples received higher scores than the uncompressed samples, unlike the rest of the donors. After 30 minutes of compression this profile remains sustained.

Donor 1, the youngest and only male donor, had a unique response to compression. In both analyses, PCA and ASCA, the 15 minute samples differed from the other two groups, demonstrating a unique sensitivity to compression. However, the response differed from the other donors as the 15 minute compressed samples were not further along the time axes than the uncompressed samples. Donor 1's uncompressed samples were the furthest along the time axes across all samples, suggesting their metabolism had a profile similar to compressed chondrocytes. This might have been interrupted when compression began and recovered as it went on.

We computed reaction rates for central energy metabolism (Fig. 1) that are consistent with each donors observed metabolic profiles (Fig. 5B). The reaction rates computed from the median metabolite values from donors 1 and 2 cluster independently, indicating that within-donor variations were greater than compression-induced variations for these two donors.

We also computed the rates that would result in a sample moving along the compression axes. All donors except donors 1 and 2 have rates similar to these. Glycolysis is prominent in these profiles, resulting in ATP and pyruvate synthesis. Also prominent is synthesis of alanine (ASde) from an aspartate precursor. Aspartate is synthesized from fumarate, which is synthesized from malate (TCA 7-8). TCA cycle malate is restored via pyruvate (AP2), indicating that overall the cell is geared toward alanine synthesis. Pyruvate and alanine are protein precursors, and an increase in protein synthesis is consistent with our previous study conducted on SW1353 chondrosarcoma (Salinas et al 2017). The data also show that compression induces a higher abundance of glutamine in the agarose-encapsulated chondrocyte samples. However, glutamate abundance also increases over time, though at a much lower rate. Glutamine may be an essential amino acid to chondrocytes(Handley et al 1980); the media contained glutamine, suggesting that the glutamine increase may also be due to transportation into the chrondrocytes rather than synthesis from glutamate. Glutamate synthesis may also be occurring due to reactions outside our model, as it is a precursor to glutathione, and chondrocytes are known to undergo oxidative stress when compressed (Brouillette et al 2014).

5 Conclusion

These results demonstrate that even grade IV osteoarthritic chondrocytes are able to respond to physiological levels of compression by synthesizing non-essential amino acids. Future studies may build on these results by using metabolic engineering to harness *in vivo* loading for cartilage repair. These analyses demonstrate the importance of using systems approaches to understand metabolomics data, as the integration of the data can yield insight that is not clear from examining metabolite values in the absence of a stoichiometric model.

6 Acknowledgements

This study was funded by the National Science Foundation (1342420 and 1554708) and the NIH (P20GM103474).

7 Conflict of Interest

The authors have received license fees from technology used in this project. The corresponding author has a financial interest in a company that licensed the metabolic flux analysis technology.

References

Alexopoulos LG, Williams GM, Upton ML, Setton LA, Guilak F (2005) Osteoarthritic changes in the biphasic mechanical properties of the chondrocyte pericellular matrix in articular cartilage. Journal of biomechanics 38(3):509–517

Blanco FJ, Rego I, Ruiz-Romero C (2011) The role of mitochondria in osteoarthritis. Nature Reviews Rheumatology 7(3):161–169

Brouillette MJ, Ramakrishnan PS, Wagner V, Sauter E, Journot B, McKinley T, Martin JA (2014) Strain-dependent oxidant release in articular cartilage originates from mitochondria. Biomechanics and modeling in mechanobiology 13(3):565–572

Coleman MC, Ramakrishnan PS, Brouillette MJ, Martin JA (2016) Injurious loading of articular cartilage compromises chondrocyte respiratory function. Arthritis & Rheumatology 68(3):662–671

Griffin TM, Huebner JL, Kraus VB, Yan Z, Guilak F (2012) Induction of osteoarthritis and metabolic inflammation by a very high-fat diet in mice: Effects of short-term exercise. Arthritis & Rheumatology 64(2):443–453

Handley C, Speight G, Leyden K, Lowther D (1980) Extracellular matrix metabolism by chondrocytes 7. evidence that l-glutamine is an essential amino acid for chondrocytes and other connective tissue cells. Biochimica et Biophysica Acta (BBA)-General Subjects 627(3):324–331

Jutila AA, Zignego DL, Hwang BK, Hilmer JK, Hamerly T, Minor CA, Walk ST, June RK (2014) Candidate mediators of chondrocyte mechanotransduction via targeted and untargeted metabolomic measurements. Archives of biochemistry and biophysics 545:116–123

Martin JA, Martini A, Molinari A, Morgan W, Ramalingam W, Buckwalter JA, McKinley TO (2012) Mitochondrial electron transport and glycolysis are coupled in articular cartilage. Osteoarthritis and cartilage 20(4):323–329

Salinas D, Minor CA, Carlson RP, McCutchen CN, Mumey BM, June RK (2017) Combining targeted metabolomic data with a model of glucose metabolism: toward progress in chondrocyte mechanotransduction. PloS one 12(1):e0168,326

Smilde AK, Jansen JJ, Hoefsloot HC, Lamers RJA, Van Der Greef J, Timmerman ME (2005) Anova-simultaneous component analysis (asca): a new tool for analyzing designed metabolomics data. Bioinformatics 21(13):3043–3048

Stephanopoulos G, Aristidou AA, Nielsen J (1998) Metabolic engineering: principles and methodologies. Academic press

Ten Berge JM, Kiers HA, Van der Stel V (1992) Simultaneous components analysis. Statistica Applicata 4(4):277–392

Timmerman ME, Kiers HA (2003) Four simultaneous component models for the analysis of multivariate time series from more than one subject to model intraindividual and interindividual differences. Psychometrika 68(1):105–121

Vallino JJ, Stephanopoulos G (1989) Flux determination in cellular bioreaction networks: applications to lysine fermentations. Frontiers in bioprocessing 1:205–219

Vincent T, McLean C, Full L, Peston D, Saklatvala J (2007) Fgf-2 is bound to perlecan in the pericellular matrix of articular cartilage, where it acts as a chondrocyte mechanotransducer. Osteoarthritis and Cartilage 15(7):752–763

Vis DJ, Westerhuis JA, Smilde AK, van der Greef J (2007) Statistical validation of megavariate effects in asca. BMC bioinformatics 8(1):322

Wilusz RE, Sanchez-Adams J, Guilak F (2014) The structure and function of the pericellular matrix of articular cartilage. Matrix biology 39:25–32

Xu X, Li Z, Cai L, Calve S, Neu CP (2016) Mapping the nonreciprocal micromechanics of individual cells and the surrounding matrix within living tissues. Scientific reports 6:24,272

Zignego DL, Jutila AA, Gelbke MK, Gannon DM, June RK (2014) The mechanical microenvironment of high concentration agarose for applying deformation to primary chondrocytes. Journal of biomechanics 47(9):2143–2148

Zignego DL, Hilmer JK, June RK (2015) Mechanotransduction in primary human osteoarthritic chondrocytes is mediated by metabolism of energy, lipids, and amino acids. Journal of biomechanics 48(16):4253–4261

```
This is pdfTeX, Version 3.14159265-2.6-1.40.16 (TeX Live 2015/W32TeX)
(preloaded format=pdflatex 2016.4.6)  11 JUN 2018 08:20
entering extended mode
 restricted \write18 enabled.
 %&-line parsing enabled.
**./v11.tex
(./v11.tex
LaTeX2e <2016/03/31>
Babel <3.9q> and hyphenation patterns for 81 language(s) loaded.

LaTeX Warning: File `example.eps' already exists on the system.
               Not generating it from this source.

(c:/TeXLive/2015/texmf-dist/tex/latex/base/fix-cm.sty
Package: fix-cm 2015/01/14 v1.1t fixes to LaTeX
(c:/TeXLive/2015/texmf-dist/tex/latex/base/ts1enc.def
File: ts1enc.def 2001/06/05 v3.0e (jk/car/fm) Standard LaTeX file
)) (c:/TeXLive/texmf-local/tex/latex/aries/svjour3.cls
Document Class: svjour3 2007/05/08 v3.2
LaTeX document class for Springer journals
(c:/TeXLive/2015/texmf-dist/tex/latex/base/fleqn.clo
File: fleqn.clo 2015/03/31 v1.1i Standard LaTeX option (flush left
equations)
\mathindent=\dimen102
Applying: [2015/01/01] Make \[ robust on input line 50.
LaTeX Info: Redefining \[ on input line 51.
Already applied: [0000/00/00] Make \[ robust on input line 62.
Applying: [2015/01/01] Make \] robust on input line 74.
LaTeX Info: Redefining \] on input line 75.
Already applied: [0000/00/00] Make \] robust on input line 83.
)
Class Springer-SVJour3 Info: extra/valid Springer sub-package (-> *.clo)
(Springer-SVJour3)           not found in option list of \documentclass
(Springer-SVJour3)           - autoactivating "global" style.
(c:/TeXLive/texmf-local/tex/latex/aries/svglov3.clo
File: svglov3.clo 2009/12/18 v3.2 style option for standardised journals
SVJour Class option: svglov3.clo for standardised journals
)
LaTeX Font Info:    Redeclaring math symbol \Gamma on input line 147.
LaTeX Font Info:    Redeclaring math symbol \Delta on input line 148.
LaTeX Font Info:    Redeclaring math symbol \Theta on input line 149.
LaTeX Font Info:    Redeclaring math symbol \Lambda on input line 150.
LaTeX Font Info:    Redeclaring math symbol \Xi on input line 151.
LaTeX Font Info:    Redeclaring math symbol \Pi on input line 152.
LaTeX Font Info:    Redeclaring math symbol \Sigma on input line 153.
LaTeX Font Info:    Redeclaring math symbol \Upsilon on input line 154.
LaTeX Font Info:    Redeclaring math symbol \Phi on input line 155.
LaTeX Font Info:    Redeclaring math symbol \Psi on input line 156.
LaTeX Font Info:    Redeclaring math symbol \Omega on input line 157.
\logodepth=\dimen103
\headerboxheight=\dimen104
\betweenumberspace=\dimen105
\aftertext=\dimen106
\headlineindent=\dimen107
```

```
\c@inst=\count79
\c@auth=\count80
\instindent=\dimen108
\authrun=\box26
\authorrunning=\toks14
\titrun=\box27
\titlerunning=\toks15
\combirun=\box28
\c@lastpage=\count81
\rubricwidth=\dimen109
\c@section=\count82
\c@subsection=\count83
\c@subsubsection=\count84
\c@paragraph=\count85
\c@subparagraph=\count86
\spthmsep=\dimen110
\c@theorem=\count87
\c@case=\count88
\c@conjecture=\count89
\c@corollary=\count90
\c@definition=\count91
\c@example=\count92
\c@exercise=\count93
\c@lemma=\count94
\c@note=\count95
\c@problem=\count96
\c@property=\count97
\c@proposition=\count98
\c@question=\count99
\c@solution=\count100
\c@remark=\count101
\c@figure=\count102
\c@table=\count103
\abovecaptionskip=\skip41
\belowcaptionskip=\skip42
\figcapgap=\dimen111
\tabcapgap=\dimen112
\figgap=\dimen113
\bibindent=\dimen114
\@tempcntc=\count104
) (c:/TeXLive/2015/texmf-dist/tex/latex/natbib/natbib.sty
Package: natbib 2010/09/13 8.31b (PWD, AO)
\bibhang=\skip43
\bibsep=\skip44
LaTeX Info: Redefining \cite on input line 694.
\c@NAT@ctr=\count105
) (c:/TeXLive/2015/texmf-dist/tex/latex/graphics/graphicx.sty
Package: graphicx 2014/10/28 v1.0g Enhanced LaTeX Graphics (DPC,SPQR)
(c:/TeXLive/2015/texmf-dist/tex/latex/graphics/keyval.sty
Package: keyval 2014/10/28 v1.15 key=value parser (DPC)
\KV@toks@=\toks16
) (c:/TeXLive/2015/texmf-dist/tex/latex/graphics/graphics.sty
Package: graphics 2016/01/03 v1.0q Standard LaTeX Graphics (DPC,SPQR)
(c:/TeXLive/2015/texmf-dist/tex/latex/graphics/trig.sty
```

```
Package: trig 2016/01/03 v1.10 sin cos tan (DPC)
) (c:/TeXLive/2015/texmf-dist/tex/latex/latexconfig/graphics.cfg
File: graphics.cfg 2010/04/23 v1.9 graphics configuration of TeX Live
)
Package graphics Info: Driver file: pdftex.def on input line 95.
(c:/TeXLive/2015/texmf-dist/tex/latex/pdftex-def/pdftex.def
File: pdftex.def 2011/05/27 v0.06d Graphics/color for pdfTeX
(c:/TeXLive/2015/texmf-dist/tex/generic/oberdiek/infwarerr.sty
Package: infwarerr 2010/04/08 v1.3 Providing info/warning/error messages
(HO)
) (c:/TeXLive/2015/texmf-dist/tex/generic/oberdiek/ltxcmds.sty
Package: ltxcmds 2011/11/09 v1.22 LaTeX kernel commands for general use
(HO)
)
\Gread@gobject=\count106
))
\Gin@req@height=\dimen115
\Gin@req@width=\dimen116
) (c:/TeXLive/2015/texmf-dist/tex/latex/amsmath/amsmath.sty
Package: amsmath 2016/03/10 v2.15b AMS math features
\@mathmargin=\skip45
For additional information on amsmath, use the `?' option.
(c:/TeXLive/2015/texmf-dist/tex/latex/amsmath/amstext.sty
Package: amstext 2000/06/29 v2.01 AMS text
(c:/TeXLive/2015/texmf-dist/tex/latex/amsmath/amsgen.sty
File: amsgen.sty 1999/11/30 v2.0 generic functions
\@emptytoks=\toks17
\ex@=\dimen117
)) (c:/TeXLive/2015/texmf-dist/tex/latex/amsmath/amsbsy.sty
Package: amsbsy 1999/11/29 v1.2d Bold Symbols
\pmbraise@=\dimen118
) (c:/TeXLive/2015/texmf-dist/tex/latex/amsmath/amsopn.sty
Package: amsopn 2016/03/08 v2.02 operator names
)
\inf@bad=\count107
LaTeX Info: Redefining \frac on input line 199.
\uproot@=\count108
\leftroot@=\count109
LaTeX Info: Redefining \overline on input line 297.
\classnum@=\count110
\DOTSCASE@=\count111
LaTeX Info: Redefining \ldots on input line 394.
LaTeX Info: Redefining \dots on input line 397.
LaTeX Info: Redefining \cdots on input line 518.
\Mathstrutbox@=\box29
\strutbox@=\box30
\big@size=\dimen119
LaTeX Font Info:    Redeclaring font encoding OML on input line 634.
LaTeX Font Info:    Redeclaring font encoding OMS on input line 635.

Package amsmath Warning: Unable to redefine math accent \vec.

\macc@depth=\count112
\c@MaxMatrixCols=\count113
```

```
\dotsspace@=\muskip10
\c@parentequation=\count114
\dspbrk@lvl=\count115
\tag@help=\toks18
\row@=\count116
\column@=\count117
\maxfields@=\count118
\andhelp@=\toks19
\eqnshift@=\dimen120
\alignsep@=\dimen121
\tagshift@=\dimen122
\tagwidth@=\dimen123
\totwidth@=\dimen124
\lineht@=\dimen125
\@envbody=\toks20
\multlinegap=\skip46
\multlinetaggap=\skip47
\mathdisplay@stack=\toks21
LaTeX Info: Redefining \[ on input line 2739.
LaTeX Info: Redefining \] on input line 2740.
) (c:/TeXLive/2015/texmf-dist/tex/latex/graphics/color.sty
Package: color 2016/01/03 v1.1b Standard LaTeX Color (DPC)
(c:/TeXLive/2015/texmf-dist/tex/latex/latexconfig/color.cfg
File: color.cfg 2007/01/18 v1.5 color configuration of teTeX/TeXLive
)
Package color Info: Driver file: pdftex.def on input line 143.
) (c:/TeXLive/2015/texmf-dist/tex/latex/lineno/lineno.sty
Package: lineno 2005/11/02 line numbers on paragraphs v4.41
\linenopenalty=\count119
\output=\toks22
\linenoprevgraf=\count120
\linenumbersep=\dimen126
\linenumberwidth=\dimen127
\c@linenumber=\count121
\c@pagewiselinenumber=\count122
\c@LN@truepage=\count123
\c@internallinenumber=\count124
\c@internallinenumbers=\count125
\quotelinenumbersep=\dimen128
\bframerule=\dimen129
\bframesep=\dimen130
\bframebox=\box31
LaTeX Info: Redefining \\ on input line 3056.
)

! LaTeX Error: File `kbordermatrix.sty' not found.

Type X to quit or <RETURN> to proceed,
or enter new name. (Default extension: sty)

Enter file name:
! Emergency stop.
<read *>
```

```
l.63 \newcommand
                {\red}[1]{{\color{red}#1}}^^M
*** (cannot \read from terminal in nonstop modes)


Here is how much of TeX's memory you used:
 2662 strings out of 493027
 36293 string characters out of 6137679
 93843 words of memory out of 5000000
 6227 multiletter control sequences out of 15000+600000
 3640 words of font info for 14 fonts, out of 8000000 for 9000
 1141 hyphenation exceptions out of 8191
 27i,0n,33p,237b,150s stack positions out of
5000i,500n,10000p,200000b,80000s
!  ==> Fatal error occurred, no output PDF file produced!
```

F1

Click here to download Figure Fig1.eps

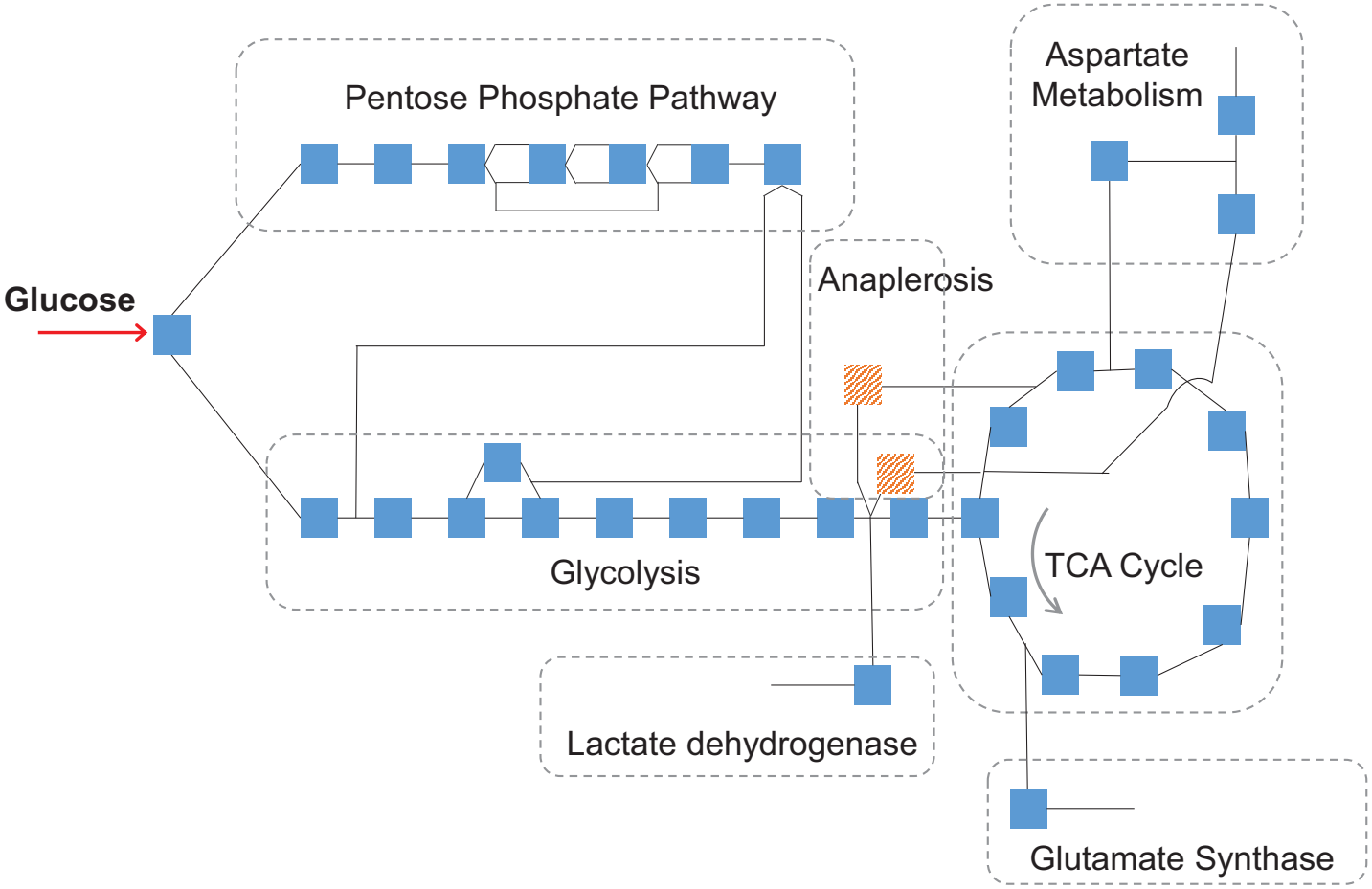

F2

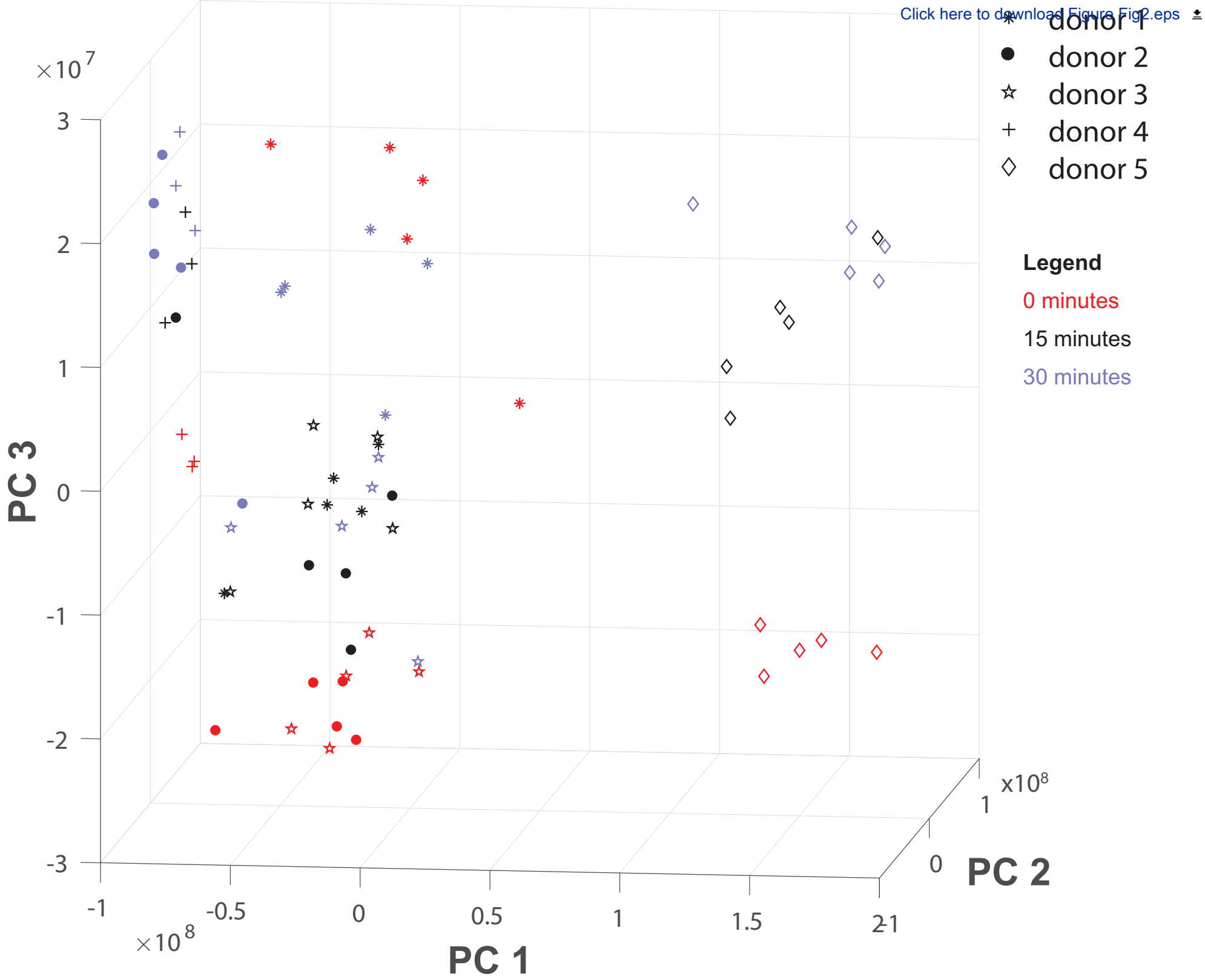

F3

Click here to download Figure Fig3.eps

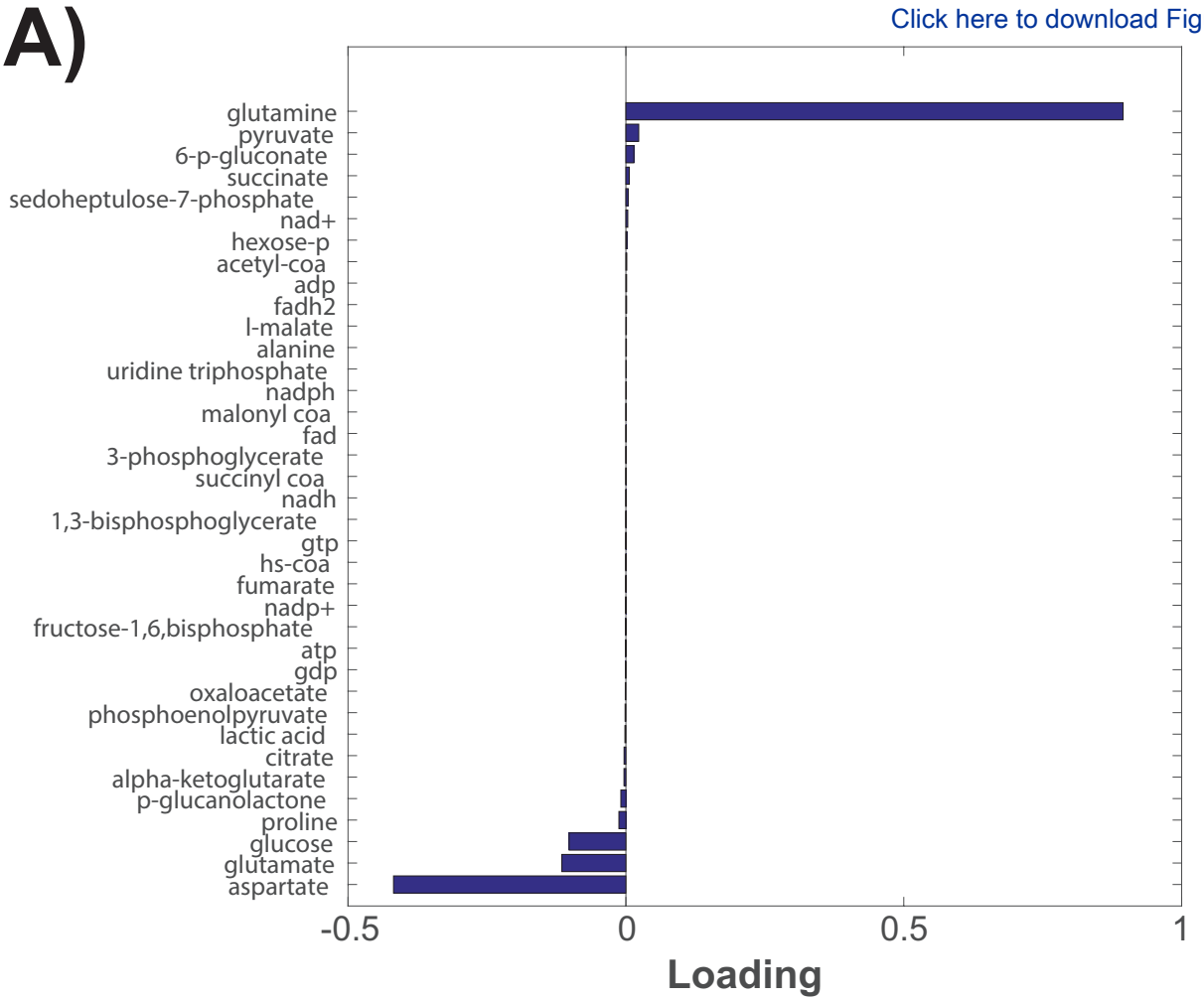

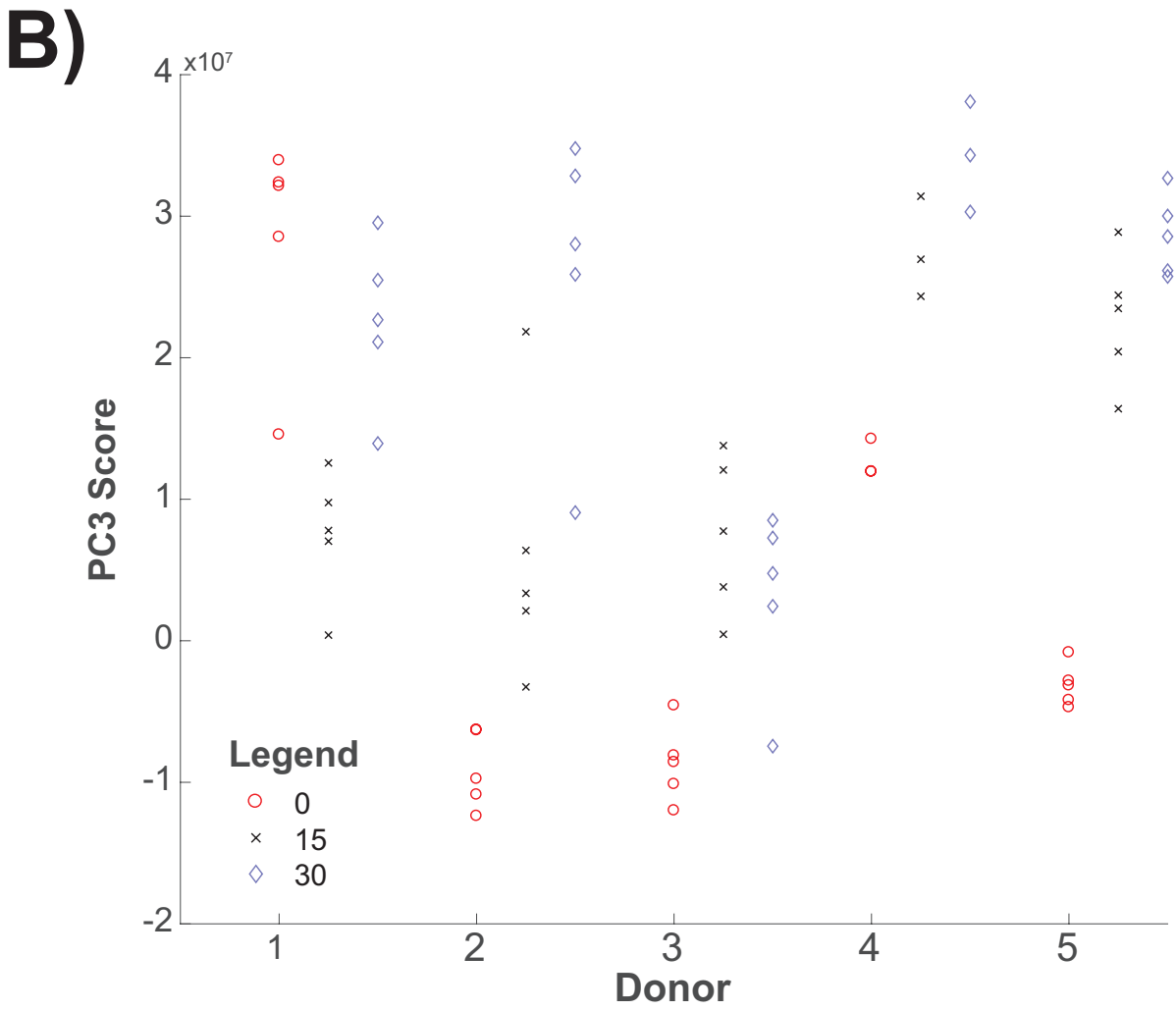

F4

Click here to download Figure Fig4.eps

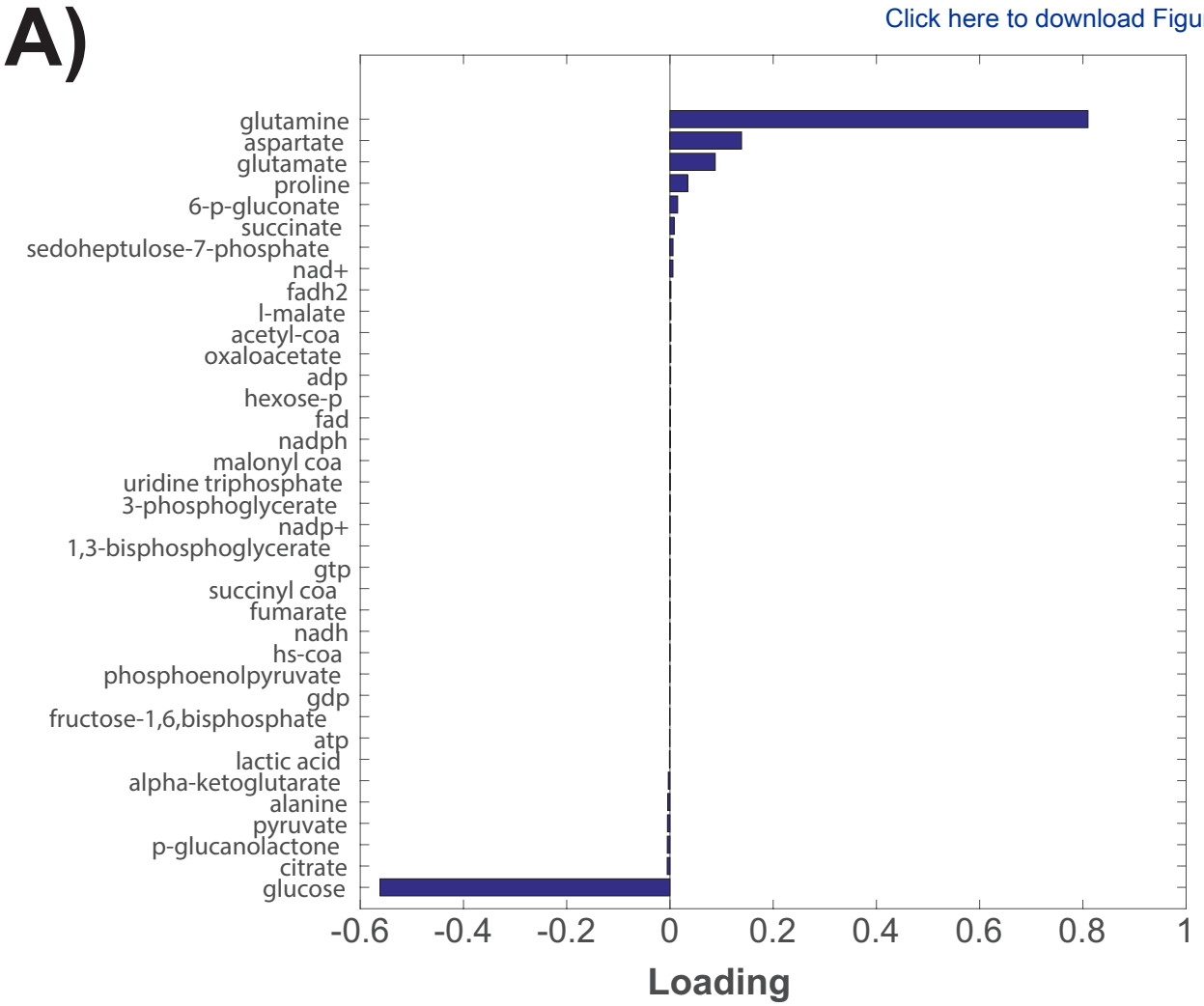

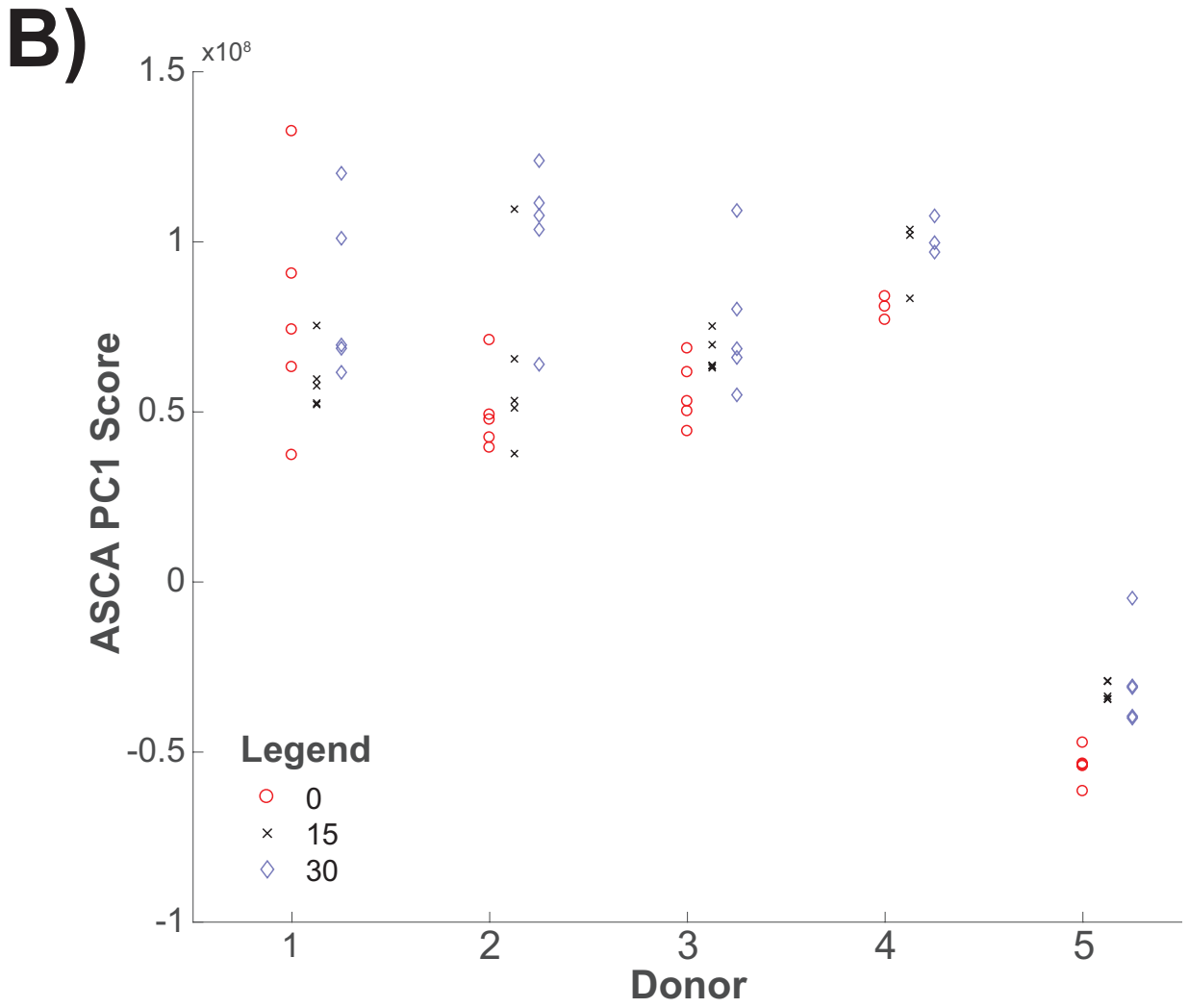

F5

Click here to download Figure Fig5.eps

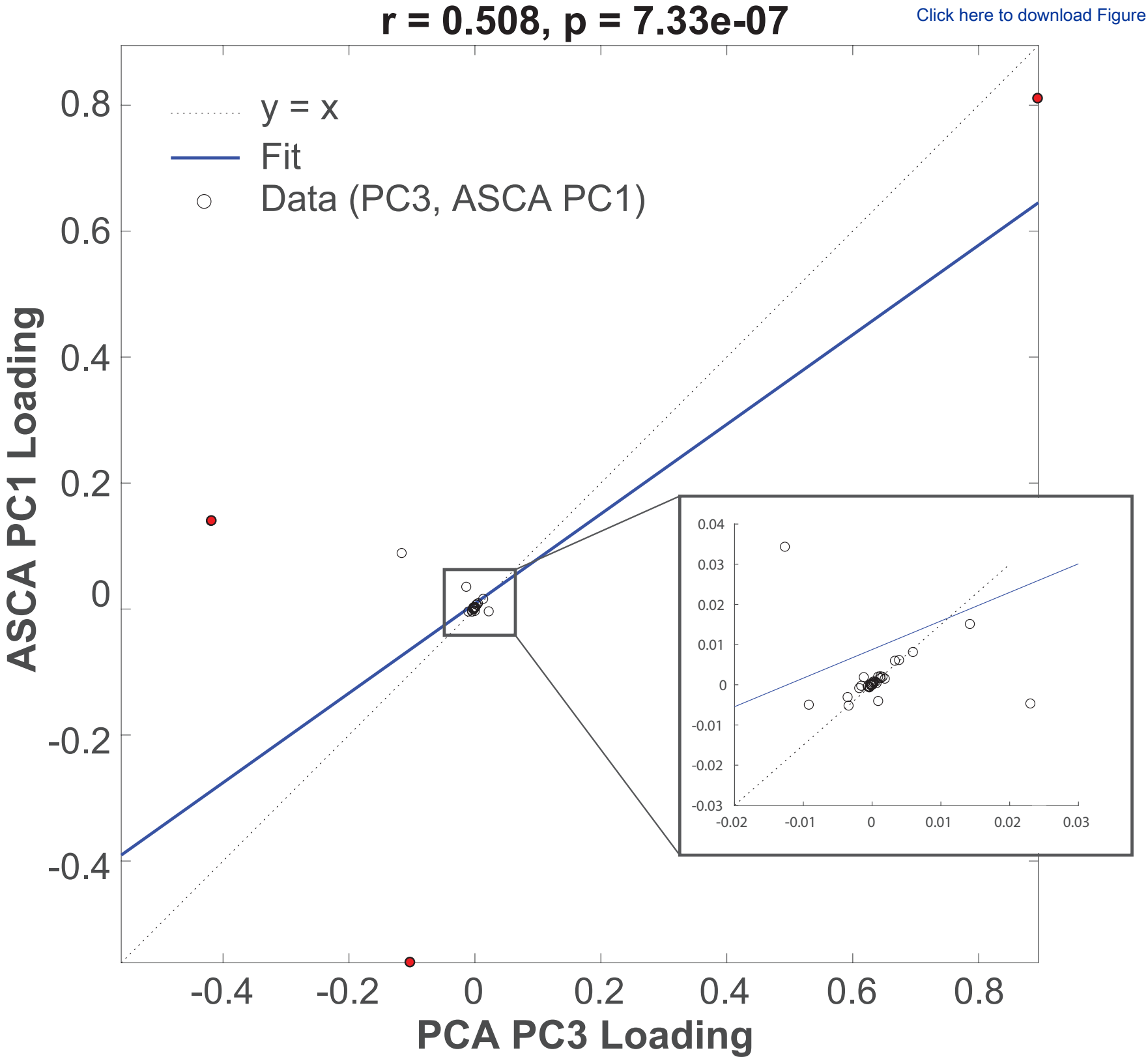

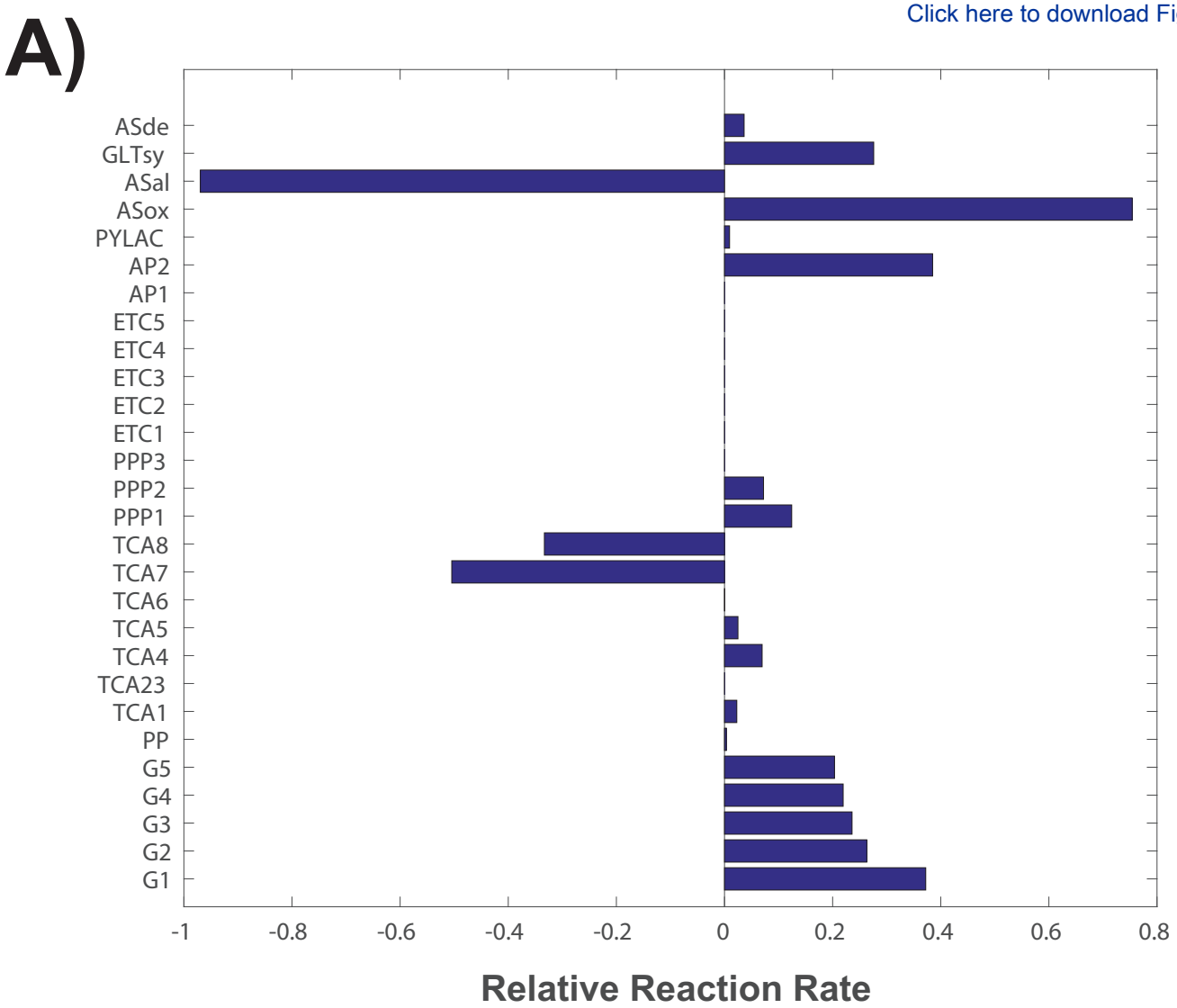

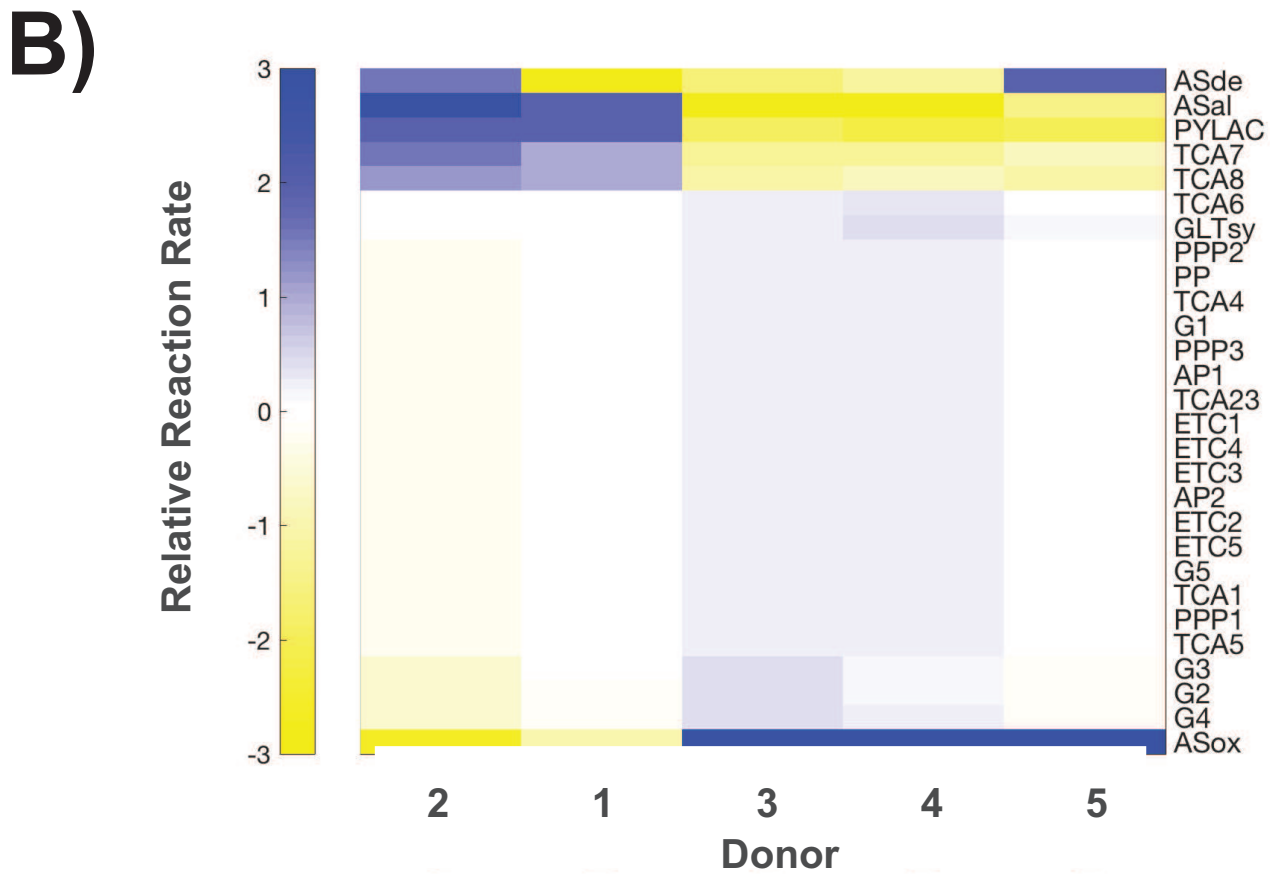

F7

Click here to download Figure Fig7.eps

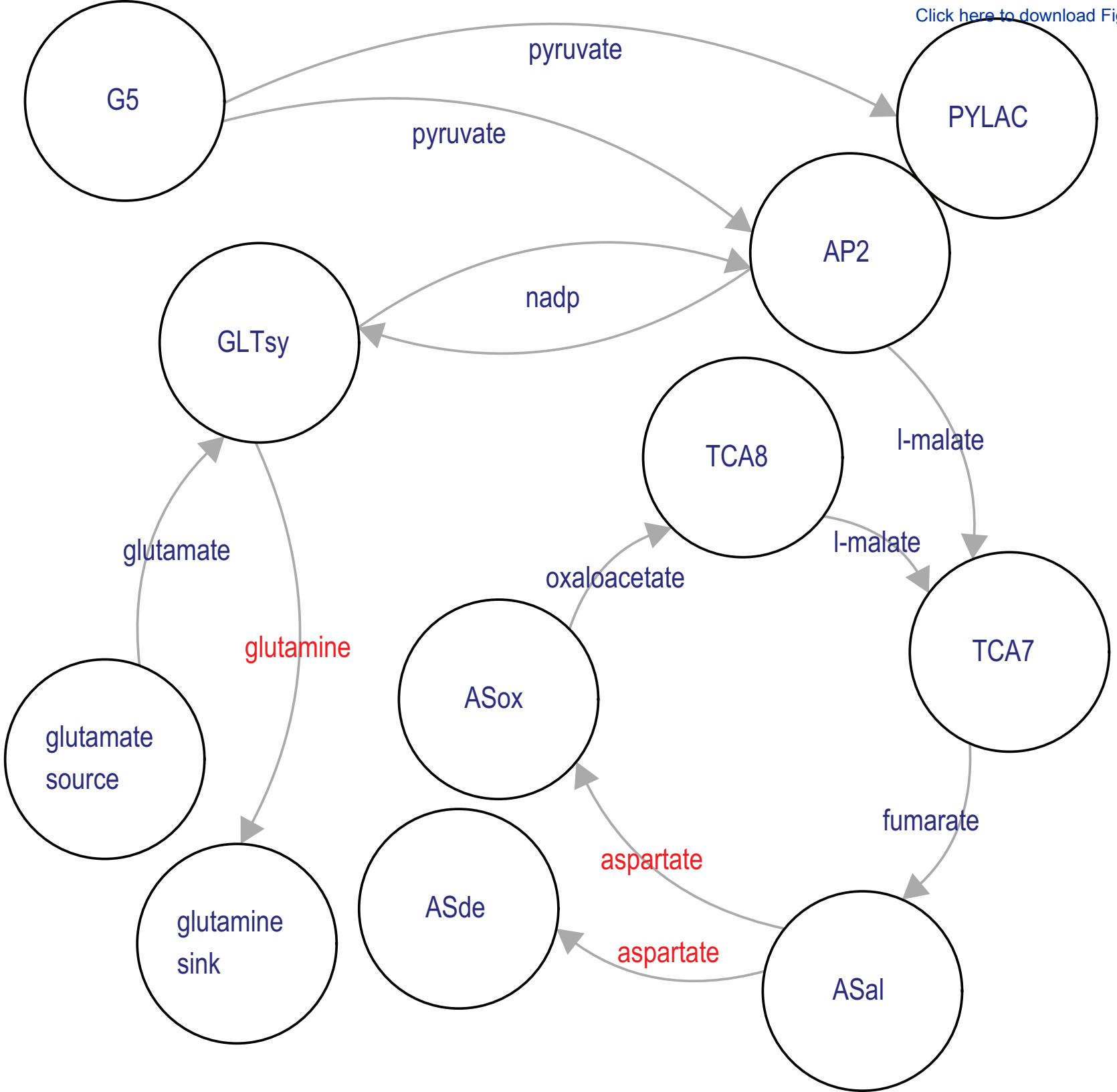

	C015	C1530
G1	0.99999992	1.00000006
G2	-8258.91981	-6739.10903
G3	-7307.54601	-6788.26349
G4	-8103.71642	-15412.0661
G5	1.00000017	0.99999988
PP	0.99999581	0.99998899
TCA1	1.00000419	1.000011
TCA23	1	1
TCA4	0.99999645	1.0000029
TCA5	-890.057572	176.731744
TCA6	-1477.13246	-7423.0518
TCA7	11246.0756	-150447.08
TCA8	37991.4248	-214651.174
PPP1	0.99999996	1.00000003
PPP2	0.99999999	1
PPP3	0.99999993	1.00000006
ETC1	1	1
ETC2	1.00000001	1
ETC3	1	1
ETC4	1	1
ETC5	1.00000004	0.99999997
AP1	0.99999996	1.00000003
AP2	1	1
PYLAC	52008.5795	-456128.296
ASox	-124511.153	409609.078
ASal	28251.0721	-284602.745
GLTsy	-6500.67994	16399.7955
ASde	-326090.713	48701.4298

	C015	C1530
G1	1.00000046	0.99999977
G2	-2886.0435	-1328.47551
G3	-3853.34075	-1453.94381
G4	-7265.91565	-1156.61738
G5	0.99999908	1.0000002
PP	1.00000567	1.00000057
TCA1	0.99999023	0.9999992
TCA23	1.00000409	1.00000009
TCA4	1.00003844	1.00000174
TCA5	28.8167141	2602.43951
TCA6	1745.53175	1497.08055
TCA7	-8345.12981	-124506.706
TCA8	1464.37927	-71535.0395
PPP1	1.00000019	0.99998915
PPP2	1.00000005	1.00001094
PPP3	1.00000042	0.99999917
ETC1	1	1
ETC2	0.99999998	1
ETC3	1	1
ETC4	1	1
ETC5	0.99999977	0.99999992
AP1	1.00000023	1.00000002
AP2	1	0.99999993
PYLAC	-23117.4063	-143151.327
ASox	90075.226	173977.14
ASal	-21866.4851	-255237.804
GLTsy	17059.5477	-1095.15533
ASde	104343.299	-46146.9891

	C015	C1530
G1	0.99999923	1.00000028
G2	-3233.88012	9086.98047
G3	-4074.84876	9163.01887
G4	2082.98422	7520.11761
G5	1.00000155	0.99999945
PP	1.00000704	1.00014422
TCA1	0.99999295	0.9998558
TCA23	1	1.00000001
TCA4	1.00000181	1.00014545
TCA5	-2618.49176	499.411941
TCA6	-4279.85314	-4866.38205
TCA7	253425.576	-41879.0016
TCA8	248188.969	-37616.5309
PPP1	0.99999959	1.00000014
PPP2	1.00000002	1
PPP3	0.99999923	1.00000028
ETC1	1	1
ETC2	1	0.99999997
ETC3	1	1
ETC4	1	1
ETC5	1.00000039	0.99999986
AP1	0.99999961	1.00000014
AP2	1	1
PYLAC	475976.905	-45212.6362
ASox	-374283.344	153948.974
ASal	503266.065	-75310.4011
GLTsy	-914.992027	-1513.54508
ASde	262280.682	-120218.943

	C015	C1530
G1	0.99999996	1.00000006
G2	4588.82703	-8869.70177
G3	4536.90953	-7469.92678
G4	4384.94545	-13175.8295
G5	1.00000009	0.99999988
PP	0.99998965	1.00000452
TCA1	1.00001035	0.99999556
TCA23	1	0.99999992
TCA4	0.99998782	1.00000075
TCA5	-6127.59454	-1234.02246
TCA6	13737.9308	2572.00912
TCA7	46734.7938	100114.637
TCA8	-18159.093	107417.862
PPP1	1.00000576	1.00000003
PPP2	0.99999422	1
PPP3	0.99999995	1.00000007
ETC1	1	1
ETC2	0.99999997	0.99999999
ETC3	1	1
ETC4	1	1
ETC5	1.00000002	0.99999997
AP1	0.99999998	1.00000003
AP2	1	1
PYLAC	-14629.8161	198855.3
ASox	76895.0307	-98227.7673
ASal	74950.9706	196074.098
GLTsy	3295.07014	2663.07203
ASde	123091.865	-418783.864

	C015	C1530
G1	1.00000061	1.00000136
G2	24958.2591	-18374.2305
G3	25134.7146	-19208.1691
G4	26044.0467	-4928.6874
G5	0.99999878	0.99999728
PP	1.00002703	1.00000935
TCA1	0.99997297	0.99999065
TCA23	1	1
TCA4	1.00002637	1.00000259
TCA5	-1119.11506	849.673807
TCA6	5631.12392	14791.9521
TCA7	-257971.774	-196783.547
TCA8	-236393.166	-141147.615
PPP1	1.00000031	1.00000062
PPP2	1	1.00000006
PPP3	1.00000061	1.00000134
ETC1	1	1
ETC2	1	0.99999993
ETC3	1	1
ETC4	1	1
ETC5	0.99999969	0.99999932
AP1	1.00000031	1.00000068
AP2	1	1
PYLAC	-376812.052	-331224.477
ASox	451747.929	347465.79
ASal	-528720.835	-425641.594
GLTsy	-919.610236	19342.9632
ASde	-324258.2	-185159.933

	PCA_Rates
G1	0.13174535
G2	0.07699895
G3	0.06322769
G4	0.0705439
G5	0.07868783
PP	0
TCA1	0.03844445
TCA23	0
TCA4	0.08617969
TCA5	0.02513742
TCA6	-0.01138915
TCA7	-0.26130647
TCA8	-0.19345327
PPP1	0
PPP2	0.0117078
PPP3	0
ETC1	-1.17E-16
ETC2	3.47E-18
ETC3	-1.34E-16
ETC4	-6.46E-17
ETC5	-4.20E-16
AP1	0
AP2	0.2502815
PYLAC	-0.05889342
ASox	0.57627717
ASal	-0.38632011
GLTsy	0.33600002
ASde	0.11457325

	ASCA_Rates
G1	0.37222394
G2	0.26328625
G3	0.23591179
G4	0.21950934
G5	0.20343581
PP	0.00352939
TCA1	0.02273579
TCA23	0
TCA4	0.06959133
TCA5	0.02491197
TCA6	0.00044245
TCA7	-0.5045317
TCA8	-0.33322589
PPP1	0.1242892
PPP2	0.0721847
PPP3	0
ETC1	-4.08E-16
ETC2	7.73E-18
ETC3	-4.60E-16
ETC4	-2.18E-16
ETC5	-1.45E-15
AP1	0
AP2	0.38493961
PYLAC	0.00935864
ASox	0.75412158
ASal	-0.96958824
GLTsy	0.27600518
ASde	0.03626307

Click here to view linked References

	PC_1	PC_2	PC_3
1,3-bisphosphoglycerate	-1.29E-05	-5.21E-06	5.02E-05
3-phosphoglycerate	-5.10E-05	-5.77E-05	0.000187941
6-p-gluconate	0.001821176	-0.001391675	0.01432814
acetyl-coa	0.000456332	-0.000122136	0.001628334
adp	0.000258937	-0.000887303	0.00134333
alpha-ketoglutarate	0.000315687	0.013334946	-0.003449894
alanine	-0.000142454	5.91E-05	0.000992521
aspartate	-0.195550159	0.874726689	-0.418111038
atp	4.62E-05	-0.000359601	-0.000288743
citrate	0.003230833	-0.001561853	-0.003306977
fructose-1,6,bisphosphate	-0.000474939	0.002407895	-0.000238332
fad	0.00018054	-0.000301692	0.000301528
fadh2	0.000543424	0.000134348	0.001320799
fumarate	3.17E-05	7.72E-05	-6.62E-05
gdp	0.000142556	-0.000206438	-0.000520027
glucose	0.979482365	0.172890876	-0.10210463
glutamate	-0.046077798	0.098055945	-0.115147566
glutamine	0.014362234	0.441179981	0.89465684
gtp	2.38E-05	-8.62E-05	-5.60E-05
hexose-p	-0.000192085	-0.000839776	0.001957648
hs-coa	2.59E-05	6.72E-05	-6.32E-05
lactic acid	-0.000397098	0.001450028	-0.001760329
l-malate	-0.000374135	0.001126837	0.000994366
malonyl coa	6.86E-05	-4.32E-05	0.00035077
nad+	0.000467954	-0.000530221	0.003426307
nadh	0.00033374	-0.000232437	0.00011464
nadp+	1.62E-05	3.01E-05	-0.000133584
nadph	0.000288784	6.73E-06	0.000589636
oxaloacetate	-0.00136537	0.003746469	-0.001099003
p-glucanolactone	-0.001863979	0.005688027	-0.009087466
phosphoenolpyruvate	4.67E-05	0.001575418	-0.001467492
proline	-0.004870621	0.017045091	-0.012570477
pyruvate	-0.000328103	0.013140424	0.023120661
sedoheptulose-7-phosphate	-6.18E-05	0.001144417	0.004031082
succinate	0.00055719	0.000548811	0.006048285
succinyl coa	0.000155672	-9.97E-05	0.000126376
uridine triphosphate	-1.96E-06	5.96E-05	0.000760319

	ASCA_PC_1	ASCA_PC_2
1,3-bisphosphoglycerate	-4.37E-05	2.34E-05
3-phosphoglycerate	0.000230774	-0.000223597
6-p-gluconate	0.014942464	0.000829501
acetyl-coa	0.001821153	-0.00024133
adp	0.001473264	0.002068005
alpha-ketoglutarate	-0.003236779	0.016780592
alanine	-0.004217122	0.006875742
aspartate	0.138723404	0.878039385
atp	-0.000828916	0.000881727
citrate	-0.005364288	0.006617657
fructose-1,6,bisphosphate	-0.000647489	-0.001353371
fad	0.000625118	0.000173285
fadh2	0.001912907	6.63E-05
fumarate	-0.000120139	-9.69E-05
gdp	-0.000619667	0.002577655
glucose	-0.561661421	0.447360598
glutamate	0.087711734	-0.012626625
glutamine	0.809905879	0.159364696
gtp	-6.89E-05	4.79E-05
hexose-p	0.001340115	-0.000742562
hs-coa	-0.000356256	9.11E-05
lactic acid	-0.000997053	0.004496722
l-malate	0.001847806	0.001806142
malonyl coa	0.000363841	6.53E-05
nad+	0.005795491	-0.002610208
nadh	-0.000197462	-0.000691599
nadp+	-1.47E-05	0.000274995
nadph	0.000570316	-0.000562598
oxaloacetate	0.001718032	0.002378701
p-glucanolactone	-0.005137738	0.005010698
phosphoenolpyruvate	-0.000427093	0.001911939
proline	0.034163158	0.049540894
pyruvate	-0.004841081	0.02063427
sedoheptulose-7-phosphate	0.005980203	0.002979639
succinate	0.007976867	0.00404725
succinyl coa	-0.000110914	-0.00048263
uridine triphosphate	0.000244681	-0.000222722